Hexokinase–mitochondrial interactions regulate glucose metabolism differentially in adult and neonatal cardiac myocytes

Guillaume Calmettes,[1,2] Scott A. John,[1,2] James N. Weiss,[1,2,3] and Bernard Ribalet[1,2,3]

[1]UCLA Cardiovascular Research Laboratory, [2]Department of Medicine (Cardiology), and [3]Department of Physiology, David Geffen School of Medicine at UCLA, Los Angeles, CA 90095

In mammalian tumor cell lines, localization of hexokinase (HK) isoforms to the cytoplasm or mitochondria has been shown to control their anabolic (glycogen synthesis) and catabolic (glycolysis) activities. In this study, we examined whether HK isoform differences could explain the markedly different metabolic profiles between normal adult and neonatal cardiac tissue. We used a set of novel genetically encoded optical imaging tools to track, in real-time in isolated adult (ARVM) and neonatal (NRVM) rat ventricular myocytes, the subcellular distributions of HKI and HKII, and the functional consequences on glucose utilization. We show that HKII, the predominant isoform in ARVM, dynamically translocates from mitochondria and cytoplasm in response to removal of extracellular glucose or addition of iodoacetate (IAA). In contrast, HKI, the predominant isoform in NRVM, is only bound to mitochondria and is not displaced by the above interventions. In ARVM, overexpression of HKI, but not HKII, increased glycolytic activity. In neonatal rat ventricular myocytes (NVRM), knockdown of HKI, but not HKII, decreased glycolytic activity. In conclusion, differential interactions of HKI and HKII with mitochondria underlie the different metabolic profiles of ARVM and NRVM, accounting for the markedly increased glycolytic activity of NRVM.

The Journal of General Physiology

INTRODUCTION

Hexokinase (HK) is the gateway enzyme of glucose metabolism, phosphorylating glucose to glucose-6-phosphaste (G-6-P) as the first step in the glycolytic, glycogen synthesis, and pentose phosphate pathways. In addition, HK is an important regulator of cell death (Vyssokikh and Brdiczka, 2003; Robey and Hay, 2005; Pastorino and Hoek, 2008). The HK family is comprised of four isoforms (HKI–IV). HKI and HKII are the most abundant isoforms, with HKI ("the brain HK") found in most tissues, but especially brain and red blood cells (Lowry and Passonneau, 1964; Purich and Fromm, 1971), where glycolysis plays a critical role. HKII ("the muscle HK"), however, is found primarily in insulin-sensitive tissues such as adipocytes and adult skeletal and cardiac muscle (Aubert-Foucher et al., 1984; Burcelin et al., 1993; Depre et al., 1999), where it accounts for ∼80% of total HK activity (Mandarino et al., 1995).

Shortly after birth, cardiac myocytes switch from predominant expression of HKI and the glucose transporter GLUT1 to the insulin-sensitive isoforms HKII and GLUT4. This switch coincides with the development of insulin sensitivity and shift from a straight carbohydrate to a mixed fat/carbohydrate diet (Postic et al., 1994). Thus, in adult cardiac cells, fatty acids are the main substrate between meals, whereas during meals when high glucose and insulin are present, glucose also becomes an important substrate for oxidative metabolism (Depre et al., 1999).

In noncardiac proliferating tumor cells, Wilson and others (Rose and Warms, 1967; Gottlob et al., 2001; Wilson, 2003; Majewski et al., 2004; Galluzzi et al., 2008; Miyamoto et al., 2008; Gimenez-Cassina et al., 2009) have suggested that HKI and HKII have different roles related to their intracellular location and regulatory properties, with HKI being primarily associated with mitochondria to deliver G-6-P to the catabolic glycolytic pathway and the tricarboxylic acid cycle (TCA) cycle. HKII fulfills a similar function when bound to mitochondria, but also translocates to the cytoplasm, where it preferentially directs G-6-P to glycogen synthesis and (presumably) other anabolic pathways. They showed biochemically that the interaction of HKII with mitochondria was not static, but was dynamically regulated by factors such as extracellular glucose, intracellular G-6-P, and kinases such as Akt and GSK-3.

We have recently expressed HKI and HKII tagged with YFP in Chinese hamster ovary (CHO) cells to track

Correspondence to Bernard Ribalet: bribalet@mednet.ucla.edu; or James N. Weiss: jweiss@mednet.ucla.edu

Abbreviations used in this paper: ARVM, adult rat ventricular myocytes; CHO, Chinese hamster ovary; CI, confidence interval; Cyto B, Cytochalasin B; G-6-P, glucose-6-phosphaste; HK, hexokinase; IAA, iodoacetate; NRVM, neonatal rat ventricular myocytes; RT-PCR, reverse transcription PCR; shRNA, short hairpin RNA; TMRM, tetramethylrhodamine, methyl ester; WT, wild type.

The Rockefeller University Press $30.00
J. Gen. Physiol. Vol. 142 No. 4 425–436
www.jgp.org/cgi/doi/10.1085/jgp.201310968

their subcellular locations in real time in response to various substrates, while measuring concomitant changes in intracellular glucose using a genetically encoded intracellular glucose biosensor (John et al., 2011). These studies directly demonstrated that HKII dynamically translocates from mitochondria, where it directs glucose catabolically toward glycolysis, to the cytoplasm, where it directs glucose anabolically toward glycogen synthesis; consistent with the Wilson hypothesis, such translocation occurs in response to changes in glucose, iodoacetate (IAA), or Akt signaling. In contrast, under all of the same conditions, HKI remained strongly associated with mitochondria to promote glycolysis (John et al., 2011). Collectively, a picture has emerged whereby HKI is single-purposed, remaining predominantly bound to mitochondria, where its primary role is to facilitate glycolysis, although under some specific nonphysiological conditions it may contribute to glycogen synthesis (Cifuentes et al., 2008). HKII, however, plays a multifunctional role: channeling G-6-P into the glycogen and anabolic pathways such as the pentose phosphate shunt when present in the cytoplasm, and preferentially shuttling G-6-P to glycolysis and oxidative phosphorylation when bound to mitochondria (Rose and Warms, 1967; Sui and Wilson, 1997; Gottlob et al., 2001; Majewski et al., 2004; Pastorino et al., 2005; Skaff et al., 2005; Galluzzi et al., 2008; Jurczak et al., 2008; Miyamoto et al., 2008; Gimenez-Cassina et al., 2009).

These findings from tumor cell lines, which are well-known to have altered glycolytic metabolism (the Warburg effect), raise the question of whether differential roles of HK isoforms are also important in physiologically normal tissues. To examine this question, we investigated whether the profoundly higher glycolytic activity of neonatal hearts compared with adult hearts may be related to their differences in HK isoform expression, using a set of novel genetically encoded optical imaging tools to track, in real-time in living neonatal and adult cardiac myocytes, the subcellular distributions of HKI and HKII, as well as the functional consequences on glucose utilization.

MATERIALS AND METHODS

Ethical approval

This study was approved by the UCLA Chancellor's Animal Research Committee (ARC 2003-063-23B) and performed in accordance with the Guide for the Care and Use of Laboratory Animals published by the United States National Institutes of Health (National Institutes of Health Publication No. 85-23, revised 1996) and with UCLA Policy 990 on the Use of Laboratory Animal Subjects in Research (revised 2010).

Neonatal and adult rat ventricular myocyte culture

Neonatal rat ventricular myocytes (NRVM) were enzymatically isolated by standard methods (Rohr et al., 1991). In brief, hearts harvested from 2–3-d-old neonatal Sprague-Dawley rats were digested with collagenase (0.02%; Worthington Biochemical Corporation) and pancreatin (0.06%; Sigma-Aldrich). Myocytes were isolated with the use of a Percoll (GE Healthcare) gradient and plated on 35-mm glass-bottom culture dishes. Adult rat ventricular myocytes (ARVM) were enzymatically isolated from the heart of 3–4-mo-old male Fisher rats as described previously (Goldhaber et al., 1989). In brief, after administering anesthesia, hearts were removed and perfused retrogradely at 37°C in Langendorff fashion with nominally Ca^{2+}-free Tyrode's buffer containing 1.2 mg/ml collagenase type II (catalog No. 4176; Worthington Biochemical Corporation) and 0.12 mg/ml protease type XIV (catalog No. P5147; Sigma-Aldrich) for 25–28 min. After washing out the enzyme solution, hearts were subsequently removed from the perfusion apparatus and gently agitated to dissociate the myocytes. The Ca^{2+} concentration was gradually increased to 1.8 mmol/liter over 30 min. This procedure typically yielded 40–60% of rod-shaped, Ca^{2+}-tolerant myocytes that were then plated on 35-mm glass-bottom culture dishes. NRVM and ARVM were cultured in DMEM high (25 mM) glucose medium supplemented with 6% (vol/vol) FBS, 100 U/ml penicillin, 100 U/ml streptomycin, and 2 mM glutamine.

Solutions and experimental techniques

The bath solution for cell imaging consisted of (in mM) 140 NaCl, 5 KCl, 1.1 $MgCl_2$, 2.5 $CaCl_2$, and 10 HEPES, with the pH adjusted to 7.2 with KOH. Glucose was added to this solution, and for the 0 glucose solution *N*-methyl-D-glucamine (NMDG) was added to maintain the solution's osmolarity. Solutions were perfused directly over the cells using a gravity fed eight way perfusion device (Warner Instruments) with electrically controlled solenoids (The Lee Company). Input and output of solution volumes to the recording chamber (35-mm glass-bottomed culture dish) were equilibrated to maintain constant flow rates and pressures within the recording chamber. Experiments were performed at room temperature (25°C). Cytochalasin B (Cyto B), Akt Inhibitor IV, and other chemicals were purchased from Sigma-Aldrich.

Plasmids constructs and transduction

We obtained the FLIPglu-600 µM cDNA from W.B. Frommer (Carnegie Institution for Science, Stanford, CA), GLUT from D. Abel (University of Utah, Salt Lake City, UT), and rat HKI and HKII from J. Wilson. Fusion of rat HKs to YFP was accomplished by inserting a Bam H1 site at the last amino acid of the coding sequence and subcloning into a modified pEYFPN-1 vector (Takara Bio Inc.). The modified pEYFPN-1 carried the mutations Q86K and A206K. All constructs were subcloned into the mammalian expression vectors using the cytomegalovirus (CMV) promoter.

Overexpression of FLIPglu-600 µM, HKI, and HKII in NRVM and ARVM was achieved with engineered adenoviruses encoding the constructs. Expression of the constructs was sufficiently high after 36–48 h (NRVM) and 72–96 h (ARVM) to perform FRET experiments or microscopy imaging.

RNA interference with short hairpin RNA (shRNA)

Biologically active shRNAs were generated from the pLKO.1-puro vector system (Naldini et al., 1996; Zufferey et al., 1997). The shRNA target sequences for HKI and HKII were purchased from Thermo Fischer Scientific. The pLKO.1-scramble (Addgene) was used as a control for RNA interference. To accomplish transgene incorporation into lentiviral capsids, pLKO.1 vectors were cotransfected with pSPAX.2 packaging vector (encoding HIV Gag, pol, and Rev proteins) in combination with pMD2.G (encoding VSV-G glycoprotein) into HEK293T cells plated on 6-cm dishes using Lipofectamine 2000. The medium was then replaced with complete DMEM containing 10% FBS, and the virus-containing supernatants were harvested 48, 72, and 96 h after transfection. All virus stocks were filtered at 0.45 µm, aliquoted, and stored at −80°C.

Immunoblot analysis

For immunoblot analyses, cells were lysed in a buffer containing 50 mM Tris, pH 7.5, 1% Triton X-100, 150 mM NaCl, 10% glycerol, and 1 mM EDTA. Samples were separated on 10% SDS-PAGE. Proteins were transferred to nitrocellulose membranes and subsequently analyzed by immunoblotting with the relevant antibodies. Antibodies used were anti-actin (clone I-19), anti-HKI (clone G-1), and anti-HKII (clone 45.6), all purchased from Santa Cruz Biotechnology, Inc. Chemiluminescence images were acquired using an Image Reader LAS-3000 LCD camera (Fujifilm). Band intensities were quantified using National Institutes of Health ImageJ software.

G-6-P assay

A commercial kit (Biovision Research Products) was used for the G-6-P assay. NRVM grown to near confluence ($2–3 \times 10^6$) were incubated in the absence of glucose or with 100 µM IAA for periods of time ranging from 0 to 25 min. After the incubation cells were washed in ice-cold PBS and frozen in situ in dry ice ethanol. 200 µl of 6% (vol/vol) perchloric acid was then added and the cells scraped while frozen. Cells were homogenized via a "Qiashredder" column at 4°C and the homogenate neutralized with 500 mM ethanolamine and 10 M KOH (Taylor et al., 2006). Samples were then centrifuged to remove insoluble material (10 min, 15,000 *g* at 4°C). 50-µl samples were transferred into wells of a 96-well plate and brought to a volume of 100 µl with assay buffer. Absorbance at 450 nm was measured, using a POLARstar Omega microplate reader (BMG LABTECH GmbH). To estimate the G-6-P levels a curve was generated with G-6-P standards containing 0, 2, 4, 6, 8, 10, and 20 nmol/well.

FRET imaging

All cells were imaged live without fixation. Images (16-bit) were acquired using a microscope (Eclipse TE300; Nikon) fitted with a 60× (1.4 NA) oil immersion lens (Nikon) and equipped with a filter cube comprising a CFP band-pass excitation filter, 436/20b, together with a longpass dichroic mirror (455DCLP; Chroma Technology Corp). LEDs (Philips Lumileds) were used as light sources: one emitting at 455 ± 20 nm (royal blue) and the other emitting at 505 ± 15 nm (cyan). LEDs and camera exposure were controlled by MetaFluor Imaging 6.1 software (Molecular Devices). Ratiometric FRET measurements were monitored from the YFP and CFP images acquired simultaneously using a Dual View image splitter (Optical Insights) equipped with a 505-nm longpass dichroic filter to separate the CFP and YFP signals, a CFP emission filter (480/30), and a YFP emission filter (535/40) (John et al., 2008, 2011). Images were captured with a Cascade 512B digital camera (Photometrics). Exposure times were optimized in each case but varied between 300–500 ms and were recorded at a constant rate for each cell between 0.2 and 0.33 Hz. Many experiments lasted >1 h, leading to a slow drift in the FRET ratio baseline in some cases.

Standard and confocal microscopy imaging

Standard microscopy images were acquired using an inverted microscope (IX70; Olympus) fitted with an Olympus Plan-Apochromat 60×, 1.4 NA oil immersion objective lens and a cooled charge-coupled device (CCD) camera (Quantix; Photometrics). Imaging Workbench software was used for data acquisition and analysis. YFP (XF104-2) and CFP (XF130-2) filter cubes were purchased from Omega Optical, Inc.

Confocal images were acquired using an inverted microscope (Axiovert 100 LSM; Carl Zeiss) fitted with a 60× water immersion objective lens (C-Apochromat 63/1.2 W Corr; Carl Zeiss). Pascal 5 image software (Carl Zeiss) was used for data acquisition and analysis.

Data analysis

Analysis of images and FRET data were implemented in the Python programming language (van Rossum and Drake, 2001), using the Numpy and Scipy packages that provide support for array manipulation and general scientific computation, respectively (Oliphant, 2007).

Translocation of HKs from mitochondria to cytoplasm was quantified by measuring the spatial variance in fluorescence over time. Because mitochondria are discrete organelles, the spatial variance is large when HK fluorescence arises predominantly from mitochondria, and decreases as HK is released and diffuses evenly through the cytoplasm (see the example in Fig. S1). The variance operator is a local neighborhood operation that calculates the sum of square of the brightness differences from the mean for the neighborhood surrounding each pixel in the original image (Russ, 2011). The variance value is small in regions of the image with uniform brightness and becomes large whenever sharp dark-bright transitions occur. In our algorithm, for each pixel in the input image, the variance was calculated for a 9-by-9 to 15-by-15 group of surrounding pixels, using the following formula:

$$\sigma^2_{window} = \frac{\sum_{i=1}^{n} x_i^2}{n} - \frac{\left(\sum_{i=1}^{n} x_i^2\right)}{n^2},$$

where x and n are, respectively, the intensity of each pixel and the number of pixel within the window.

FRET ratio recovery after glucose removal was analyzed by data fitting to the sigmoid function:

$$y = a + \frac{b-a}{1+\exp^{(x_0-x)/s}},$$

where x_0, an estimate of the time requires to reach half of the change in FRET ratio, accounts for the lag period, whereas s, an estimate of the rate of change, is more or less independent of the lag period. a and b are, respectively, the lower and upper asymptotes of the sigmoid function.

Statistical analysis

For each dataset, the mean and accompanying 95% confidence intervals (CIs) are reported. The conventional percentile bootstrap-resampling approach with 10,000 replications was used for estimating 95% CI as well as examining the significant difference between groups (effect size statistics; Efron and Tibshirani, 1991; Nakagawa and Cuthill, 2007; Calmettes et al., 2012). A P-value <0.05 was considered statistically significant. All analyses were performed by subroutines for bootstrapping developed in the Python programming language (van Rossum and Drake, 2001), using the Numpy and Scipy packages, based on the code we previously published (Calmettes et al., 2012).

Online supplemental material

Fig. S1 shows principles of spatial variance–based image analysis. Fig. S2 shows IAA-induced changes in G6P as a function of time in NRVM. Fig. S3 shows a quantification of HKI and HKII overexpression in NRVM infected by HKI and HKII adenoviruses. Fig. S4 shows a quantification of the differential expression of GLUT and HK isoforms in neonatal and adult hearts. Fig. S5 shows effects of IAA on NRVM glycolytic activity measured using the FRET glucose sensor. Fig. S6 shows effects of 0 glucose and IAA on intracellular pH in CHO cells, and the effects of cytosolic acidification on HKII translocation in NRVM. Fig. S7 shows calibration of the FRET glucose sensor used to calculate the rates of glucose utilization in cardiac myocytes. Online supplemental material is available at http://www.jgp.org/cgi/content/full/jgp.201310968/DC1.

RESULTS

HK subcellular localization in AVRM and NRVM

To assess the subcellular localization of HKI and HKII in cardiac myocytes, we used confocal microscopy to image living ARVM and NRVM infected with YFP-tagged HKI or HKII, using an adenoviral vector. To determine whether HKs colocalized with mitochondria, the infected cells were also loaded with 30 nM tetramethylrhodamine, methyl ester (TMRM), a widely used marker of the mitochondrial network. Typical images obtained from ARVM and NRVM expressing HK-YFP isoforms (green pseudo-color) and loaded with TMRM (red pseudo-color) are presented in Fig. 1 (A and B, respectively). As shown in this figure, there is almost perfect overlap (yellow) between the images obtained with HKI-YFP and the corresponding TMRM images. This observation suggests that HKI colocalizes with mitochondria in both ARVM and NRVM. In contrast, HKII appeared to colocalize with mitochondria to some extent, but was also found throughout the cytoplasm, as indicated by the presence of diffuse green in the merged images. These results agree with our data previously obtained in CHO cells (John et al., 2011), confirming the hypothesis that these properties of HK isoforms are not unique to tumor cells, but also occur in native tissue.

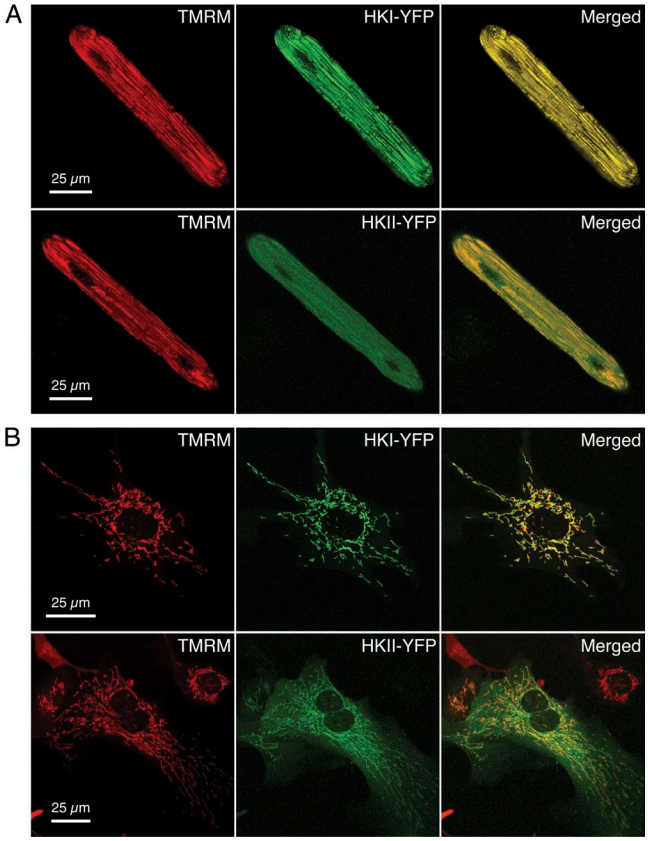

Figure 1. Subcellular distribution of HKI and HKII linked to YFP in ARVM and NRVM. Confocal images of an ARVM (A) and a NRVM (B) overexpressing HKI and HKII tagged with YFP (green) and loaded with TMRM (red). Merged YFP and TMRM images show complete colocalization of HKI with mitochondria (yellow color), but only partial colocalization of HKII, with the remainder diffusely present through the cytoplasm. Confocal images were acquired half-way through the height of the myocyte in the z direction.

HK translocation in ARVM versus NRVM

We have previously shown that removal of glucose, exposure to the glycolytic inhibitor IAA, or expression of constitutively active Akt all regulate HK distribution in CHO cells (John et al., 2011). Here we investigated how these interventions affect the subcellular distribution of HKI and HKII in ARVM and NRVM. For these experiments, time-lapsed confocal images of HKI-YFP and HKII-YFP fluorescence were compared with the corresponding TMRM images of the mitochondrial network in the same cell, using a customized image-processing algorithm that calculated the spatial variance in HK-YFP and TMRM fluorescence (see Materials and methods for details and Fig. S1). This analysis provides accurate measurements of HK redistribution between the mitochondrial and cytoplasm compartments over time (Fig. S1), but does not provide absolute levels of HK binding to the various intracellular compartments, in part because of the nonuniformity of their structures. In ARVM, the subcellular distribution of HKII-YFP was sensitive to extracellular glucose (Fig. 2). In the presence of glucose, a large fraction of HKII was bound to mitochondria, and upon removal of glucose, HKII rapidly translocated to the cytosol, with a time constant averaging 9.8 min (95% CI [8.4, 11.3], $n = 7$; Fig. 2 D). In contrast, the mitochondrial pattern of HKI-YFP fluorescence did not change significantly when extracellular glucose was removed even after 40 min (Fig. 3). This was quantified by a lack of change in the spatial variance of YFP fluorescence (Fig. 3, C and D; $n = 6$). These results show that in ARVM, HKI binding to mitochondria is very stable, whereas HKII binding is labile and dynamically regulated by extracellular glucose.

However, in NRVM, both HKI and HKII remained associated with mitochondria upon glucose removal (Fig. 4, A and B, white and light gray traces; $n = 8$ and $n = 15$, respectively). Because (1) Akt is known to facilitate HKII interaction with mitochondria (Miyamoto et al., 2008) and (2) we previously demonstrated that overexpression of constitutively active Akt in CHO cells prevented HKII translocation from mitochondria to cytoplasm in response to glucose removal (John et al., 2011), we speculated that the higher affinity of HKII to mitochondria in NRVM could be caused by high endogenous Akt activity. However, preincubation of NRVM for 1 h with Akt-inhibitor IV (10 µM) did not facilitate HKII dissociation when glucose was removed (Fig. 4 B, dark gray trace; $n = 6$), making this possibility unlikely. Furthermore, treatment with IAA to inhibit glycolysis

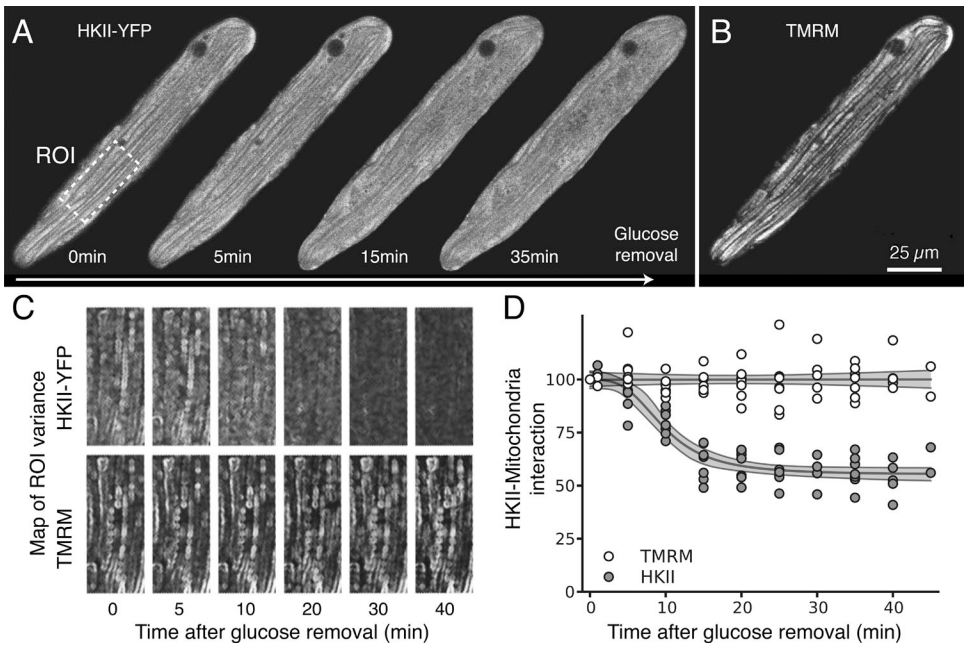

Figure 2. Glucose removal induces dissociation of HKII from mitochondria in ARVM. (A) The images obtained with adenoviral HKII-YFP construct expressed in ARVM show that 5–10 min after glucose removal, HKII progressively dissociated from mitochondria. (B) By comparison, the TMRM signal labeling the mitochondrial network was not affected by removal of glucose, even after 30 min. (C) Translocation of HKII from mitochondria to cytoplasm was quantified by computing the spatial variance of the fluorescence over time (see Materials and methods for details and Fig. S1). After glucose removal, the spatial variance of the HKII-YFP image decreased over time, showing that HKII is released and diffuses evenly through the cytoplasm. In contrast, no change in variance is observed in TMRM fluorescence (internal control). (D) Changes (percentage of control) in spatial variance of HKII-YFP (gray dots) and TMRM (white dots) during glucose removal, which indicates HKII dissociation from mitochondria. Fit of the data (gray lines), from which the time constant of dissociation can be calculated (see Results). The corresponding shaded gray areas represent 95% CIs of the fit model.

and promote intracellular G-6-P accumulation (Fig. S2) readily caused HKII redistribution from mitochondria to cytoplasm in NRVM (Fig. 4, C and D; $n = 10$).

Basal glucose handling in ARVM and NRVM

It has been reported that the HKI/HKII ratio is higher in neonatal heart than in adult heart (Postic et al., 1994), which is consistent with mRNA expression levels measured with reverse transcription PCR (RT-PCR; (Fig. S4). In addition, our data presented in the previous section indicate that HKI has a stronger binding affinity to mitochondria than HKII (Figs. 1–4). Thus, NRVM are expected to use glucose at a higher rate than ARVM, as mitochondria-bound HK is more glycolytically

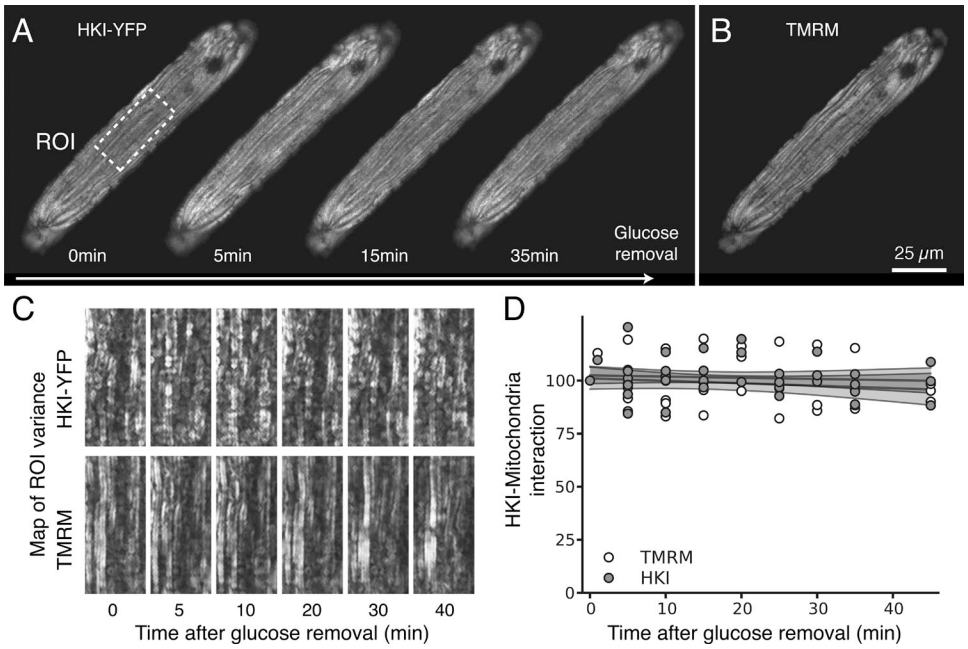

Figure 3. Glucose removal does not affect HKI interaction with mitochondria in ARVM. (A) In contrast to Fig. 2, images obtained with ARVM expressing an adenoviral HKI-YFP construct show that removal of glucose had no effect on HKI binding to mitochondria, which suggests that HKI has a much stronger binding affinity for mitochondria compared with HKII in ARVM. (B) TMRM image of the corresponding mitochondrial network after 30 min of glucose removal. (C and D) Spatial variance (see Materials and methods for details and Fig. S1) of HKI-YFP and TMRM at various time points after glucose removal, revealing the lack of effect of glucose removal on HKI's interaction with mitochondria. Gray lines in D show the fit of the data, with surrounding shaded gray areas representing 95% CIs of the fit model.

active compared with cytoplasmic HK (Southworth, 2009; John et al., 2011). To test this hypothesis, we measured basal and dynamic glucose handling in ARVM and NRVM in response to varying extracellular glucose concentrations, using the FRET-based glucose sensor FLIPglu-600 μM inserted into an adenoviral vector to measure glucose utilization. In the Results section, we have used half-times to quantify and report the dynamic changes in intracellular glucose, but in addition, we have calibrated the FRET glucose sensor to estimate the rates of glucose entry and utilization (Fig. S7). Fig. 5 (A and B) illustrates typical recordings of the YFP/CFP emission ratios obtained in ARVM and NRVM under comparable experimental conditions. In the absence of extracellular glucose, the baseline FRET ratio was lower in AVRM ($n = 14$) than in NRVM ($n = 8$), averaging 1.3 (95% CI [1.2, 1.4]) and 2.3 (95% CI [2.1, 2.5]), respectively. This difference, which was statistically significant ($P < 0.01$; Fig. 5 D), suggests that the resting intracellular glucose concentration is significantly higher in ARVM than NRVM, which is consistent with enhanced glycolytic activity of NRVM. This is consistent with the data presented in the next section where overexpression of HKI in ARVM, but not in NRVM, further increases the FRET ratio (i.e., lowered intracellular glucose).

When extracellular glucose concentration was increased from 0 to 10 mM, the YFP/CFP emission ratio decreased, reflecting glucose entry into the cell (Fig. 5, A and B). Upon removal of extracellular glucose, the ratio returned to its original value, indicating clearance of intracellular glucose by the combined effects of glucose efflux through GLUT transporters and glucose metabolism (Fehr et al., 2003; John et al., 2008). To compare the rate of glucose metabolism, independently from its efflux, in NVRM and ARVM, we used Cyto B (20 μM) to block GLUT-sensitive trans-membrane glucose transport (John et al., 2011). The metabolism of glucose could then be estimated from the half-time of intracellular glucose clearance obtained by fitting the

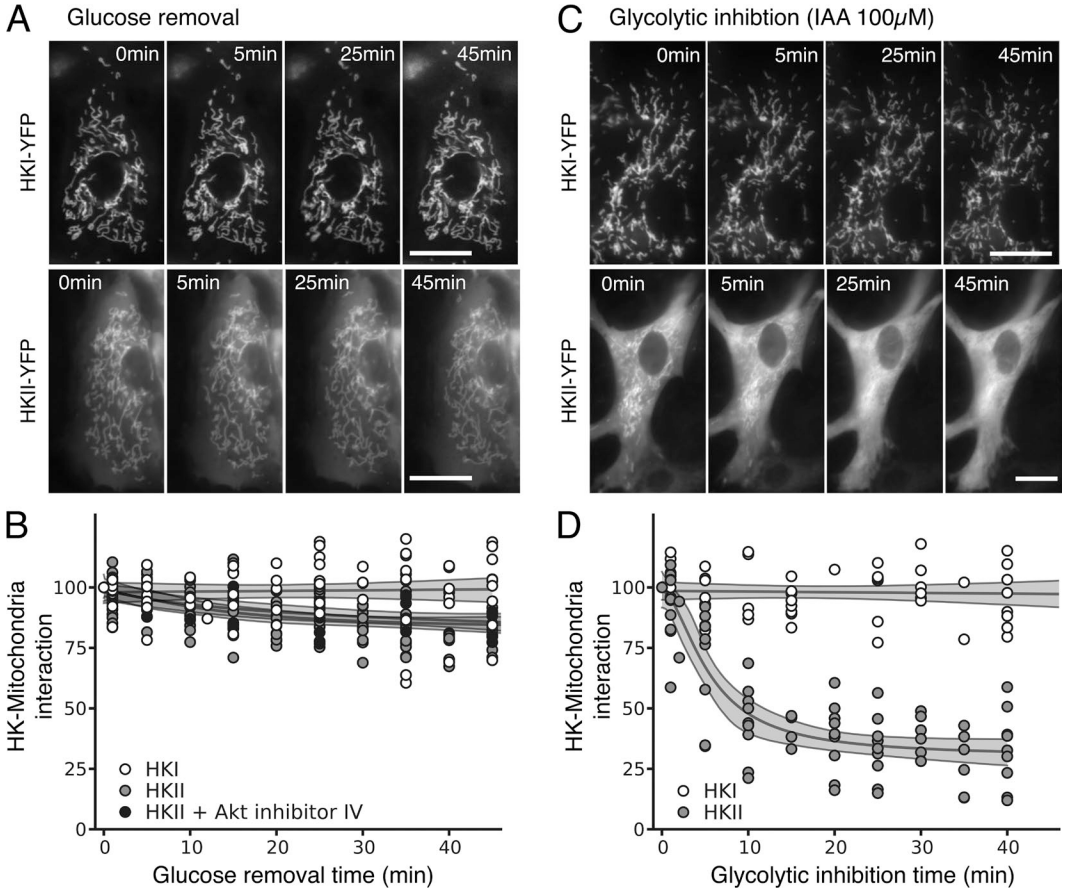

Figure 4. Effects of glucose removal, IAA and Akt inhibition on HKI, and HKII binding to mitochondria in NRVM. (A) Images of NRVM expressing the adenoviral HKI-YFP (top) and HKII-YFP (bottom) construct during glucose removal. (B) Quantitative spatial variance of HKI-YFP and HKII-YFP images reveals that HKI binding to mitochondria is insensitive to glucose removal in NRVM, whereas in contrast to ARVM, HKII hardly dissociates in NRVM. Inhibition of Akt did not make HKII more dissociable during glucose removal. (C) Images of NRVM expressing the adenoviral HKI-YFP (top) and HKII-YFP (bottom) construct during glycolytic inhibition with IAA. Bars, 25 μm. (D) Quantitative spatial variance of HKI-YFP and HKII-YFP images shows that IAA caused the dissociation of HKII from mitochondria to cytoplasm, but doesn't have any effect on HKI.

data with a sigmoidal curve (see Materials and methods for details). An example of sigmoidal fits obtained for AVRM and NRVM is shown in Fig. 5 C (traces labeled 1 and 2 in panels A and B, respectively).

In ARVM (n = 7), exposure to the GLUT inhibitor Cyto B dramatically decreased the rate of glucose clearance upon glucose removal (Fig. 5 A), with the half-time increasing by +432 s (95% CI [386, 474]) (i.e., an 8.1-fold increase, 95% CI [7.1, 9.1]). This observation indicates that in ARVM, GLUT-mediated glucose efflux, rather than glycolysis, is the dominant factor regulating glucose clearance. In contrast, addition of Cyto B in NRVM (n = 13) had almost no effect on the rate of glucose clearance after glucose removal (Fig. 5 B). This result suggests that glucose metabolism, rather than glucose efflux, dominates glucose clearance in NRVM. The striking differences in glucose handling between AVRM and NRVM are summarized in Fig. 5 E, revealing a 33.5-fold (95% CI [28.8, 40.2]) shorter half-time in the FRET ratio change associated with glucose clearance in NRVM than ARVM, which is qualitatively consistent with the reportedly fivefold higher rate of glucose consumption observed during development in neonatal ventricle (Lopaschuk et al., 1991).

Effect of HK overexpression on glucose metabolism in ARVM and NRVM

To measure how HK levels affect glucose metabolism, we overexpressed HKI-YFP and HKII-YFP in NRVM and ARVM. Our Western-blot data analysis indicates that overexpression of HKI and HKII caused a two-to-five-fold increase in HK levels (Fig. S3). In ARVM (Fig. 6 A), overexpression of HKI markedly accelerated the rate of glucose utilization measured in the presence of Cyto B (Fig. 6 A, white vs. gray traces), decreasing the half-time from 493 s (95% CI [446, 534], n = 7) to 89 s (95% CI [75 103], n = 8; Fig. 6 B). This result corresponds to an effect size of −404 s, 95% CI (−449, −356) on the half-time of glucose utilization (i.e, a 5.6-fold decrease, [4.7, 6.7]; Fig. 6 B). With this large increase in glucose clearance due to HKI overexpression, the difference in the half-time of the FRET ratio change associated with glucose clearance between AVRM and NRVM decreased to 6.0-fold (95% CI [4.7, 7.5]), a value comparable to other reports (Lopaschuk et al., 1991). As a result of increased glucose utilization, the steady-state levels of intracellular glucose decreased both in the presence and absence of outside glucose (Fig. 6 F). Thus, after overexpression of HKI the resting FRET ratio shifted from 1.32 (95% CI [1.23, 1.42]), without exogenous

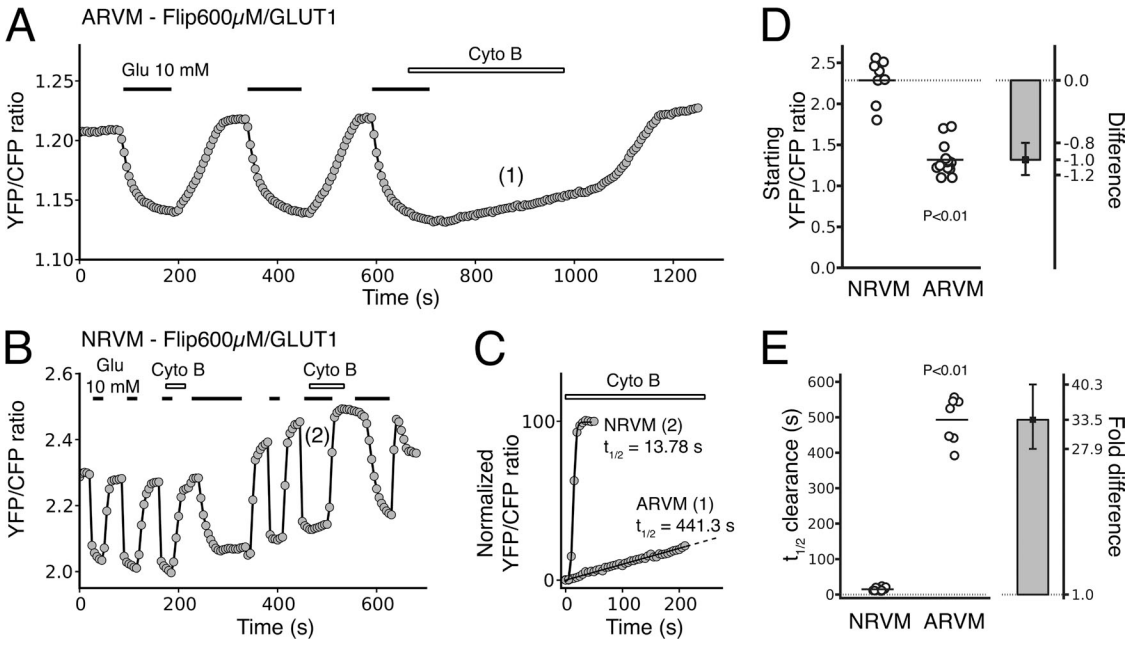

Figure 5. Glucose utilization in ARVM and NRVM. (A and B) The FRET-based glucose nanosensor Flipglu-600 μM was expressed in ARVM (A) and NRVM (B) to monitor glucose utilization in living cardiac myocytes. Superimposition of the traces in C illustrates the dramatic difference in the rate of glucose utilization in ARVM and NRVM when glucose efflux is blocked by Cyto B. (E) The dot plot reports all the individual values of half-time of the FRET ratio change associated with glucose utilization obtained in the presence of Cyto B for ARVM and NRVM. The bar plot shows the corresponding effect size (expressed as fold difference), with error bars representing the 95% CIs of that effect size. (D) The dot plot reports all the individual values of initial FRET ratio (reflecting the resting glucose concentration) obtained in ARVM and NRVM. The bar plot shows the corresponding effect size (expressed as algebraic difference), with error bars representing the 95% CIs of that effect size. The results indicate that resting intracellular glucose concentration is much lower in NRVM, which is consistent with a higher glycolytic activity. P-values reported were calculating using bootstrap resampling (see Materials and methods for details).

HKI to 1.50 (95% CI [1.43, 1.58]; P = 0.0165) with overexpressed HKI. In contrast, overexpression of HKII did not affect glucose utilization in ARVM (Fig. 6 A, black vs. gray traces), with the half-time of the FRET ratio change associated with glucose utilization remaining similar to wild-type (WT) cells (465 s, 95% CI [407, 521], $n = 9$; Fig. 6 B). As a result, steady-state intracellular glucose levels in the presence and absence of extracellular glucose were not affected by overexpression of HKII. In NRVM (Fig. 6 C), however, overexpression of HKI or HKII had no significant effect on glucose utilization rate (Fig. 6 C, white, gray, and black traces), with similar half-times of FRET ratio decline associated with glucose utilization observed for nontransfected samples (15 s, 95% CI [13, 17], $n = 13$), HKI overexpression (12 s, 95% CI [10, 15], $n = 5$), and HKII overexpression (17 s, 95% CI [13, 20], $n = 6$; Fig. 6 E). Similarly, the steady-state FRET ratio levels in the presence and absence of extracellular glucose were not affected by overexpression of either HKI or HKII.

Together with RT-PCR revealing a significantly higher HKI/HKII ratio in NRVM than ARVM (Fig. S4), these observations suggest that HKI is responsible for the very high glucose utilization rate in NRVM. This high glycolytic rate observed in NRVM is consistent with the dramatic decrease in glucose utilization observed in these cells when IAA is present (Fig. S5). To confirm these hypotheses, we investigated the effect of down-regulating the expression of HKI and HKII, using HKI or HKII shRNA (Fig. 6 D). Knockdown of HKI slowed glucose utilization in NRVM (Fig. 6 D, white vs. gray traces), resulting in a significant prolongation in the half-time of the FRET ratio change associated with glucose clearance from 15 s (95% CI [13, 17], $n = 13$) to 34 s (95% CI [30, 39], $n = 7$), i.e., a 2.3-fold decrease (95% CI [1.9, 2.8]; Fig. 6 E). In contrast, down-regulation of HKII had no effect (Fig. 6 D, gray vs. black traces), with the half-time of the FRET ratio change associated with glucose utilization remaining unchanged (12 s, 95% CI [11, 14], $n = 5$, for HKII-KO vs. 15 s, 95% CI [13, 17], $n = 13$, for WT; Fig. 6 E).

In three out of four cases where we tested the effects of overexpression of HKII in ARVM and HKI and HKII in NRVM, we did not observe any increase in the rate of FRET ratio change associated with glucose utilization,

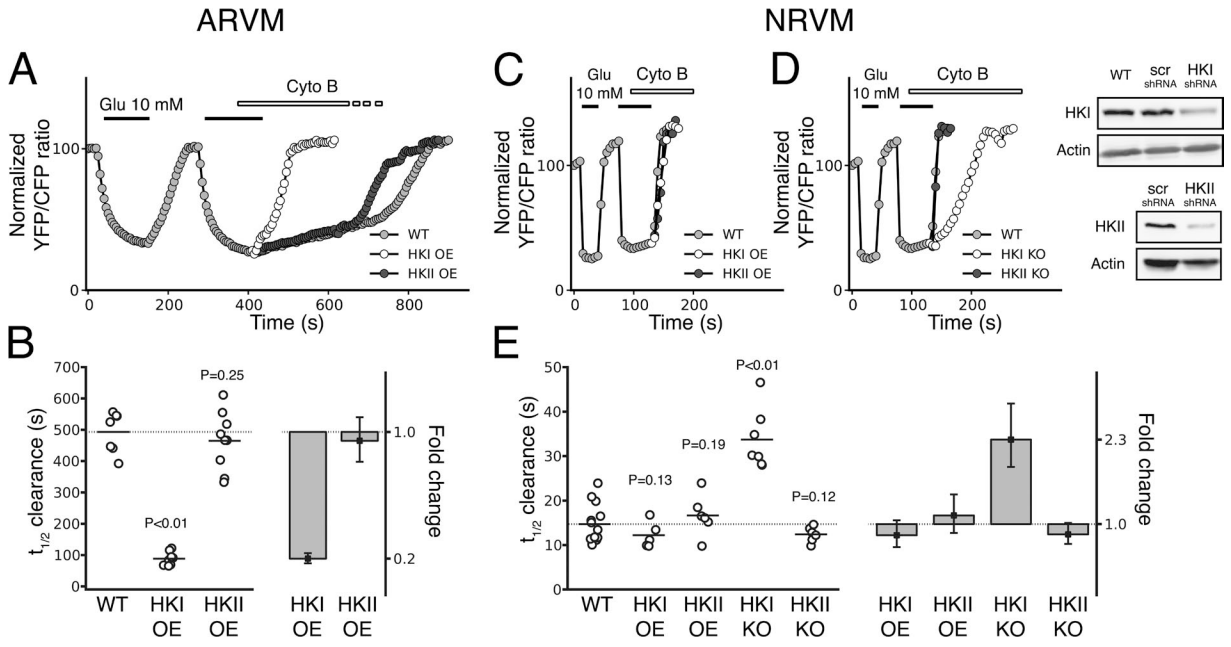

Figure 6. Effects of HKI and HKII overexpression and knockdown on glucose utilization in ARVM and NRVM. (A) In ARVM, overexpression of HKI dramatically increased the rate of glucose utilization (white) compared with control (gray), whereas overexpressing HKII had no significant effect (black). (B) All the individual half-times of the FRET ratio change associated with glucose utilization obtained for the different conditions in ARVM are represented in the dot plot. The bar plot indicates a fivefold decrease (effect size) in the half-time when HKI is overexpressed, while the values are similar to control for HKII overexpression. The error bars represents the 95% CIs of the effect size. (C) In NRVM, however, overexpression of HKI or HKII did not significantly change the half-time of the FRET ratio change associated with glucose utilization (gray, white, and black traces). (D) However, down-regulation of HKI (white), but not HKII (black), dramatically slowed the half-time in NRVM, which suggests that glucose phosphorylation is performed primarily by HKI and not HKII. Down-regulation of HKI and HKII using lentivirus shRNA were assessed by Western blotting and compared with WT and nontargeting shRNA (scr-shRNA) preparations. (E) The dot plot shows that in NRVM, the half-time of FRET ratio change associated with glucose utilization is only affected (2.3-fold increase, effect size in bar plot) when HKI is knocked down, but not by HKII knockdown (KO), or HKI and HKII overexpression (OE). P-values reported were calculated using bootstrap resampling (see Materials and methods for details).

despite a two-to-fivefold increase in protein (Fig. S3). These data together with our imaging data of HKI-YFP and HKII-YFP clearly demonstrate that our transfection of HK is highly efficient, and thus the lack of effect of exogenous HK on the rate of metabolism cannot be attributed to a lack of HK expression. Even though we were not able to get enough material to quantify the exogenous and endogenous protein levels in ARVM, our imaging data obtained with HKI-YFP and HKII-YFP clearly demonstrate that our infection protocol with the adenovirus is highly efficient. Thus, it is unlikely that the lack of effect of HKI and HKII on the rate of glucose metabolism in AVRM reflects a lack of exogenous enzyme expression.

Finally, our quantitation of HK protein levels shows that knockdown of HKI and HKII in NRVM was efficient (Fig. 6 D). Thus, again in this case the lack of effect of HKII knockdown on glucose utilization cannot be attributed to a poor depletion of endogenous HKII.

DISCUSSION

In this study, we used optical methods to track in real time the subcellular distributions of HKI and HKII in normal neonatal and adult cardiac cells, which were directly correlated with glycolytic activity under varying experimental conditions. Of the four mammalian HKs, HKI and HKII are the major cardiac isoforms, with HKII levels higher in ARVM, whereas HKI is higher in NVRM (Postic et al., 1994; Smeele et al., 2011). The RT-PCR data reported here (Fig. S4) are in agreement with these observations. Consistent with previous biochemical analyses in heart tissue (Russell et al., 1992), we show that HKI and HKII have different intracellular distributions, and directly document, for the first time, the functional consequences on regulation of glucose metabolism (catabolism vs. anabolism) in ARVM and NRVM. Given the known protective effects of HK binding to mitochondria against cell death and ischemia/reperfusion injury (Robey and Hay, 2005; Pastorino and Hoek, 2008; Smeele et al., 2011; Wu et al., 2011), it is interesting to speculate that the differential distribution of HKI and HKII may potentially contribute to the reduced susceptibility of neonatal heart to ischemia-reperfusion injury, compared with adult heart (Riva and Hearse, 1993; Ostadal et al., 1999).

In cardiac myocytes, glycolytic activity correlates with the levels of HKI and HKII

Our RT-PCR data (Fig. S4) fit with earlier results indicating that ARVM express high levels of HKII, whereas NRVM predominantly express HKI (Postic et al., 1994). Although mRNA expression levels do not always correlate with functional protein levels, our functional data using the FRET probe FLIP-Glu600 μM (Fehr et al., 2003; John et al., 2008, 2011) indicate that ARVM are less glycolytically active than NRVM, which is consistent with the observation that mitochondria-bound HKs are associated with a higher glucose phosphorylation rate. Furthermore, overexpression of HKI but not HKII increased the glycolytic rate in ARVM, whereas overexpression of HKI or HKII had little effect in NRVMs, suggesting that the activity of endogenous HKs in NRVM is near maximal. Conversely, down-regulating HKI, but not HKII, significantly reduced the glycolytic rate in NRVMs. From these data, we deduce that in AVRM (1) endogenous HKI activity is quite low, (2) little HKII is bound to mitochondria, and (3) exogenous HKII is predominantly directed to the cytosol, where it regulates glycogen synthesis and other anabolic pathways, but does not efficiently substitute for endogenous HKI to feed glycolysis. Because overexpression of HKII has no effect on the slow phase of glucose utilization when efflux is blocked in AVRM, as opposed to what was previously shown in CHO cells (John et al., 2011), we surmise that the activity of the endogenous HKII to synthesize glycogen must be near maximal. This is again consistent with our RT-PCR data. In contrast, in NRVM, the basal rate of glucose phosphorylation was very high and overexpression of HKI or HKII had no effect on the rate of glucose phosphorylation. These results indicate that the level of endogenous HKs is sufficient to stimulate glucose metabolism maximally. The observation that the inhibitor IAA caused a dramatic decrease in glucose utilization in NRVM is consistent with this hypothesis (Fig. S5).

Unfortunately, direct quantitative comparison of the rate of glucose clearance by metabolism between ARVM and NRVM was not possible, as extrapolating the half-time in FRET ratio directly to glucose consumption rate is complicated by many factors, including differences in the surface-to-volume ratio between NRVM and AVRM, the fact that NRVM were spontaneously beating and actively dividing whereas ARVM were quiescent, and the nonlinear relationship between FRET ratio and intracellular glucose concentration. For these reasons, we were not able to calibrate the half-time of the decrease in FRET ratio associated with glucose clearance directly into rates of glucose utilization in micromoles per second. However, qualitatively, the substantially shorter half-time of the FRET ratio change associated with glucose clearance via metabolism in NRVM than in ARVM is qualitatively consistent with the previously reported greater rate of glycolysis in the NRVM (Lopaschuk et al., 1991).

Translocation of HKs in NRVM is regulated by IAA, but not Akt

Previous findings have established G-6-P as an important mediator promoting HKII dissociation from mitochondria to cytosol (White and Wilson, 1990; Aleshin et al., 1998; Sebastian et al., 1999). In CHO cells overexpressing HKII, but not HKI, we found that glucose removal was associated with a delay in the subsequent

rate of glucose phosphorylation (when Cyto B was present to block glucose efflux; John et al., 2011). Based on our prior detailed analysis in CHO cells (John et al., 2011), we attribute this delay to the activation of glycogenolysis when glucose was removed, which elevated G-6-P levels to both inhibit HKII and promote its dissociation from mitochondria. This interpretation was supported by our findings that IAA, which elevates G-6-P by inhibiting glycolysis distally (Fig. S2), caused HKII to dissociate from mitochondria in intact CHO cells with glucose present, and that exogenous G-6-P accelerated dissociation of HKs from mitochondria in permeabilized CHO cells (John et al., 2011).

In the present study, we have tested the effect of glucose removal and IAA on the intracellular distribution of HKI and HKII in both AVRM and NRVM. Consistent with our findings in CHO cells, either removal of glucose or addition of IAA in the presence of glucose displaced HKII from mitochondria in AVRM, while having no effect on HKI. In NRVM, however, removal of glucose did not cause HKII to dissociate from mitochondria, although IAA in the presence of glucose did. This observation may be explained assuming that either less glycogen is synthesized in NRVM, because most HK is bound to mitochondria, or that glycogen degradation into G-6-P is a slow process in these cells. In either case, removal of glucose does not appear to raise G-6-P levels sufficiently to induce HKII dissociation from mitochondria. IAA, however, permits glucose phosphorylation but blocks glycolysis downstream, leading to G-6-P accumulation (Fig. S2), which causes HKII to dissociate from mitochondria.

It was recently suggested that G-6-P-induced HKII translocation from ARVM mitochondria outer membrane required an acidic pH_i (<7.0; Pasdois et al., 2012). This possibility warranted further investigation, as it was also recently found that removal of extracellular glucose may cause a decrease in intracellular pH from 7.4 to 7.0 in live Neuro2A cells (Tantama et al., 2011). To investigate whether a change in intracellular pH is necessary to facilitate G-6-P–induced HKII translocation, we measured intracellular pH with the BCECF probe after removal of glucose or addition of IAA in CHO cells and NRVM (Fig. S6). In both cell types removal of glucose had little effect of intracellular pH, and if anything there was a slight alkalinization, due perhaps to decreased lactate production. In the case of IAA, we observed a small (<0.05 U) but transient acidification (Fig. S6). Based on these results, we conclude that in our case the elevation of G-6-P caused by IAA or glucose removal (Fig. S2) evokes HKII dissociation independently of intracellular acidification.

We also previously found that expression of constitutively active Akt in CHO cells strengthened the interaction of HKII with mitochondria so that glucose removal no longer induced its translocation to the cytosol (John et al., 2011), which is consistent with studies showing that Akt signaling enhances the binding of HKII to mitochondria (Miyamoto et al., 2008). Thus, a high level of basal Akt activity in NRVM might also explain the lack of response to glucose removal. However, this possibility is unlikely because preincubation with Akt inhibitor IV in NRVM failed to restore HKII dissociation from mitochondria in response to glucose removal. This result suggests that, in NRVM, Akt is not a primary regulator of HKII binding to mitochondria, but rather a modulator of its sensitivity to G-6-P.

In summary, our findings indicate that HKI and HKII exhibit similar properties in normal native cardiac tissue as in tumor cell lines, despite pathophysiological alterations that may be present in the latter. HKII, the predominant isoform in ARVM, dynamically distributes between the mitochondria and cytoplasm in a G-6-P–dependent manner. In contrast, HKI, the predominant isoform in NRVM remains bound to mitochondria. In ARVM, overexpression of HKI, but not HKII, increased glycolytic activity, whereas in NRVM, knockdown of HKI, but not HKII, decreased glycolytic activity. These results suggest that differing interaction of HKI and HKII with mitochondria plays a key role in defining the different metabolic profiles of ARVM and NRVM, accounting for the markedly increased glycolytic activity of NRVM. In future studies, it will be interesting to explore how these HK isoform–related effects on glucose metabolism and interactions with mitochondria may be related to the increased resistance of NRVM to ischemia-reperfusion injury. Our results may also raise caution in extrapolating findings in NRVM to the adult heart when studying conditions such as hypertrophy and heart failure in which metabolic factors have important influences.

We thank Dr. Alan Garfinkel for advice on the bootstrap resampling implementation and Drs. Sonal Srikanth, Yousang Gwack, and Pauline Morand for technical help.

This work was supported by National Institutes of Health/ National Heart, Lung, and Blood Institute (NHLBI) grants P50 HL080111, R01 HL071870, and R01 HL095663; NIH/NHLBI contract No. HHSN268201000035C (Mitochondrial Proteomics Center); and the Laubisch and Kawata Endowments. G. Calmettes was supported by a Postdoctoral J. William Fulbright Fellowship and a Postdoctoral Fellowship award (No. 11POST6110007) from the American Heart Association (Western States). B. Ribalet was supported by a Grant in Aid from the American Heart Association 13GRNT14650074 (Western States).

Edward N. Pugh Jr. served as editor.

Submitted: 22 January 2013
Accepted: 30 August 2013

REFERENCES

Aleshin, A.E., C. Zeng, G.P. Bourenkov, H.D. Bartunik, H.J. Fromm, and R.B. Honzatko. 1998. The mechanism of regulation of hexokinase: new insights from the crystal structure of recombinant human brain hexokinase complexed with glucose and glucose-6-phosphate. *Structure.* 6:39–50. http://dx.doi.org/10.1016/S0969-2126(98)00006-9

Aubert-Foucher, E., B. Font, and D.C. Gautheron. 1984. Rabbit heart mitochondrial hexokinase: solubilization and general properties.

Arch. Biochem. Biophys. 232:391–399. http://dx.doi.org/10.1016/0003-9861(84)90554-X

Burcelin, R., R.L. Printz, J. Kande, R. Assan, D.K. Granner, and J. Girard. 1993. Regulation of glucose transporter and hexokinase II expression in tissues of diabetic rats. *Am. J. Physiol.* 265:E392–E401.

Calmettes, G., G.B. Drummond, and S.L. Vowler. 2012. Making do with what we have: use your bootstraps. *J. Physiol.* 590:3403–3406. http://dx.doi.org/10.1113/jphysiol.2012.239376

Cifuentes, D., C. Martínez-Pons, M. García-Rocha, A. Galina, L. Ribas de Pouplana, and J.J. Guinovart. 2008. Hepatic glycogen synthesis in the absence of glucokinase: the case of embryonic liver. *J. Biol. Chem.* 283:5642–5649. http://dx.doi.org/10.1074/jbc.M706334200

Depre, C., J.L. Vanoverschelde, and H. Taegtmeyer. 1999. Glucose for the heart. *Circulation.* 99:578–588. http://dx.doi.org/10.1161/01.CIR.99.4.578

Efron, B., and R. Tibshirani. 1991. Statistical data analysis in the computer age. *Science.* 253:390–395. http://dx.doi.org/10.1126/science.253.5018.390

Fehr, M., S. Lalonde, I. Lager, M.W. Wolff, and W.B. Frommer. 2003. In vivo imaging of the dynamics of glucose uptake in the cytosol of COS-7 cells by fluorescent nanosensors. *J. Biol. Chem.* 278:19127–19133. http://dx.doi.org/10.1074/jbc.M301333200

Galluzzi, L., O. Kepp, N. Tajeddine, and G. Kroemer. 2008. Disruption of the hexokinase-VDAC complex for tumor therapy. *Oncogene.* 27:4633–4635. http://dx.doi.org/10.1038/onc.2008.114

Gimenez-Cassina, A., F. Lim, T. Cerrato, G.M. Palomo, and J. Diaz-Nido. 2009. Mitochondrial hexokinase II promotes neuronal survival and acts downstream of glycogen synthase kinase-3. *J. Biol. Chem.* 284:3001–3011. http://dx.doi.org/10.1074/jbc.M808698200

Goldhaber, J.I., S. Ji, S.T. Lamp, and J.N. Weiss. 1989. Effects of exogenous free radicals on electromechanical function and metabolism in isolated rabbit and guinea pig ventricle. Implications for ischemia and reperfusion injury. *J. Clin. Invest.* 83:1800–1809. http://dx.doi.org/10.1172/JCI114085

Gottlob, K., N. Majewski, S. Kennedy, E. Kandel, R.B. Robey, and N. Hay. 2001. Inhibition of early apoptotic events by Akt/PKB is dependent on the first committed step of glycolysis and mitochondrial hexokinase. *Genes Dev.* 15:1406–1418. http://dx.doi.org/10.1101/gad.889901

John, S.A., M. Ottolia, J.N. Weiss, and B. Ribalet. 2008. Dynamic modulation of intracellular glucose imaged in single cells using a FRET-based glucose nanosensor. *Pflugers Arch.* 456:307–322. http://dx.doi.org/10.1007/s00424-007-0395-z

John, S., J.N. Weiss, and B. Ribalet. 2011. Subcellular localization of hexokinases I and II directs the metabolic fate of glucose. *PLoS ONE.* 6:e17674. http://dx.doi.org/10.1371/journal.pone.0017674

Jurczak, M.J., A.M. Danos, V.R. Rehrmann, and M.J. Brady. 2008. The role of protein translocation in the regulation of glycogen metabolism. *J. Cell. Biochem.* 104:435–443. http://dx.doi.org/10.1002/jcb.21634

Lopaschuk, G.D., M.A. Spafford, and D.R. Marsh. 1991. Glycolysis is predominant source of myocardial ATP production immediately after birth. *Am. J. Physiol.* 261:H1698–H1705.

Lowry, O.H., and J.V. Passonneau. 1964. The relationships between substrates and enzymes of glycolysis in brain. *J. Biol. Chem.* 239:31–42.

Majewski, N., V. Nogueira, R.B. Robey, and N. Hay. 2004. Akt inhibits apoptosis downstream of BID cleavage via a glucose-dependent mechanism involving mitochondrial hexokinases. *Mol. Cell. Biol.* 24:730–740. http://dx.doi.org/10.1128/MCB.24.2.730-740.2004

Mandarino, L.J., R.L. Printz, K.A. Cusi, P. Kinchington, R.M. O'Doherty, H. Osawa, C. Sewell, A. Consoli, D.K. Granner, and R.A. DeFronzo. 1995. Regulation of hexokinase II and glycogen synthase mRNA, protein, and activity in human muscle. *Am. J. Physiol.* 269:E701–E708.

Miyamoto, S., A.N. Murphy, and J.H. Brown. 2008. Akt mediates mitochondrial protection in cardiomyocytes through phosphorylation of mitochondrial hexokinase-II. *Cell Death Differ.* 15:521–529. http://dx.doi.org/10.1038/sj.cdd.4402285

Nakagawa, S., and I.C. Cuthill. 2007. Effect size, confidence interval and statistical significance: a practical guide for biologists. *Biol. Rev. Camb. Philos. Soc.* 82:591–605. http://dx.doi.org/10.1111/j.1469-185X.2007.00027.x

Naldini, L., U. Blömer, P. Gallay, D. Ory, R. Mulligan, F.H. Gage, I.M. Verma, and D. Trono. 1996. In vivo gene delivery and stable transduction of nondividing cells by a lentiviral vector. *Science.* 272:263–267. http://dx.doi.org/10.1126/science.272.5259.263

Oliphant, T.E. 2007. Python for Scientific Computing. *Computing in Science and Engineering.* 9:10–20.

Ostadal, B., I. Ostadalova, and N.S. Dhalla. 1999. Development of cardiac sensitivity to oxygen deficiency: comparative and ontogenetic aspects. *Physiol. Rev.* 79:635–659.

Pasdois, P., J.E. Parker, and A.P. Halestrap. 2012. Extent of mitochondrial hexokinase II dissociation during ischemia correlates with mitochondrial cytochrome c release, reactive oxygen species production, and infarct size on reperfusion. *J. Am. Heart Assoc.* 2:e005645. http://dx.doi.org/10.1161/JAHA.112.005645

Pastorino, J.G., and J.B. Hoek. 2008. Regulation of hexokinase binding to VDAC. *J. Bioenerg. Biomembr.* 40:171–182. http://dx.doi.org/10.1007/s10863-008-9148-8

Pastorino, J.G., J.B. Hoek, and N. Shulga. 2005. Activation of glycogen synthase kinase 3beta disrupts the binding of hexokinase II to mitochondria by phosphorylating voltage-dependent anion channel and potentiates chemotherapy-induced cytotoxicity. *Cancer Res.* 65:10545–10554. http://dx.doi.org/10.1158/0008-5472.CAN-05-1925

Postic, C., A. Leturque, R.L. Printz, P. Maulard, M. Loizeau, D.K. Granner, and J. Girard. 1994. Development and regulation of glucose transporter and hexokinase expression in rat. *Am. J. Physiol.* 266:E548–E559.

Purich, D.L., and H.J. Fromm. 1971. The kinetics and regulation of rat brain hexokinase. *J. Biol. Chem.* 246:3456–3463.

Riva, E., and D.J. Hearse. 1993. Age-dependent changes in myocardial susceptibility to ischemic injury. *Cardioscience.* 4:85–92.

Robey, R.B., and N. Hay. 2005. Mitochondrial hexokinases: guardians of the mitochondria. *Cell Cycle.* 4:654–658. http://dx.doi.org/10.4161/cc.4.5.1678

Rohr, S., D.M. Schölly, and A.G. Kléber. 1991. Patterned growth of neonatal rat heart cells in culture. Morphological and electrophysiological characterization. *Circ. Res.* 68:114–130. http://dx.doi.org/10.1161/01.RES.68.1.114

Rose, I.A., and J.V. Warms. 1967. Mitochondrial hexokinase. Release, rebinding, and location. *J. Biol. Chem.* 242:1635–1645.

Russ, J.C. 2011. The Image Processing Handbook, Sixth Edition. CRC Press, Inc., Boca Raton, FL. 885 pp.

Russell, R.R. III, J.M. Mrus, J.I. Mommessin, and H. Taegtmeyer. 1992. Compartmentation of hexokinase in rat heart. A critical factor for tracer kinetic analysis of myocardial glucose metabolism. *J. Clin. Invest.* 90:1972–1977. http://dx.doi.org/10.1172/JCI116076

Sebastian, S., J.E. Wilson, A. Mulichak, and R.M. Garavito. 1999. Allosteric regulation of type I hexokinase: A site-directed mutational study indicating location of the functional glucose 6-phosphate binding site in the N-terminal half of the enzyme. *Arch. Biochem. Biophys.* 362:203–210. http://dx.doi.org/10.1006/abbi.1998.1043

Skaff, D.A., C.S. Kim, H.J. Tsai, R.B. Honzatko, and H.J. Fromm. 2005. Glucose 6-phosphate release of wild-type and mutant

human brain hexokinases from mitochondria. *J. Biol. Chem.* 280: 38403–38409. http://dx.doi.org/10.1074/jbc.M506943200

Smeele, K.M., R. Southworth, R. Wu, C. Xie, R. Nederlof, A. Warley, J.K. Nelson, P. van Horssen, J.P. van den Wijngaard, S. Heikkinen, et al. 2011. Disruption of hexokinase II-mitochondrial binding blocks ischemic preconditioning and causes rapid cardiac necrosis. *Circ. Res.* 108:1165–1169. http://dx.doi.org/10.1161/CIRCRESAHA.111.244962

Southworth, R. 2009. Hexokinase-mitochondrial interaction in cardiac tissue: implications for cardiac glucose uptake, the 18FDG lumped constant and cardiac protection. *J. Bioenerg. Biomembr.* 41:187–193. http://dx.doi.org/10.1007/s10863-009-9207-9

Sui, D., and J.E. Wilson. 1997. Structural determinants for the intracellular localization of the isozymes of mammalian hexokinase: intracellular localization of fusion constructs incorporating structural elements from the hexokinase isozymes and the green fluorescent protein. *Arch. Biochem. Biophys.* 345:111–125. http://dx.doi.org/10.1006/abbi.1997.0241

Tantama, M., Y.P. Hung, and G. Yellen. 2011. Imaging intracellular pH in live cells with a genetically encoded red fluorescent protein sensor. *J. Am. Chem. Soc.* 133:10034–10037. http://dx.doi.org/10.1021/ja202902d

Taylor, A.J., J.M. Ye, and C. Schmitz-Peiffer. 2006. Inhibition of glycogen synthesis by increased lipid availability is associated with subcellular redistribution of glycogen synthase. *J. Endocrinol.* 188:11–23. http://dx.doi.org/10.1677/joe.1.06381

van Rossum, G., and F.L. Drake. 2001. Python Reference Manual. http://docs.python.org/release/2.2/ref/ref.html (accesssed Sept. 12, 2013).

Vyssokikh, M.Y., and D. Brdiczka. 2003. The function of complexes between the outer mitochondrial membrane pore (VDAC) and the adenine nucleotide translocase in regulation of energy metabolism and apoptosis. *Acta Biochim. Pol.* 50:389–404.

White, T.K., and J.E. Wilson. 1990. Binding of nucleoside triphosphates, inorganic phosphate, and other polyanionic ligands to the N-terminal region of rat brain hexokinase: relationship to regulation of hexokinase activity by antagonistic interactions between glucose 6-phosphate and inorganic phosphate. *Arch. Biochem. Biophys.* 277:26–34. http://dx.doi.org/10.1016/0003-9861(90)90545-A

Wilson, J.E. 2003. Isozymes of mammalian hexokinase: structure, subcellular localization and metabolic function. *J. Exp. Biol.* 206:2049–2057. http://dx.doi.org/10.1242/jeb.00241

Wu, R., K.M. Smeele, E. Wyatt, Y. Ichikawa, O. Eerbeek, L. Sun, K. Chawla, M.W. Hollmann, V. Nagpal, S. Heikkinen, et al. 2011. Reduction in hexokinase II levels results in decreased cardiac function and altered remodeling after ischemia/reperfusion injury. *Circ. Res.* 108:60–69. http://dx.doi.org/10.1161/CIRCRESAHA.110.223115

Zufferey, R., D. Nagy, R.J. Mandel, L. Naldini, and D. Trono. 1997. Multiply attenuated lentiviral vector achieves efficient gene delivery in vivo. *Nat. Biotechnol.* 15:871–875. http://dx.doi.org/10.1038/nbt0997-871